

In the search of an ideal measurement geometry for effect coatings

Jiří Filip^a, Frank J. Maile^b

^a*Institute of Information Theory and Automation of the CAS, Prague, Czech Republic*

^b*Schlenk Metallic Pigments, GmbH, Roth, Germany*

Abstract

Visualization and analysis of effect coatings capturing, become highly important nowadays, when digital appearance content is necessary for facilitating quick communication of material appearance properties across various industries. The contribution of this paper is twofold. First, we discuss development of measurement geometries used in the industry, discuss limitations related to small instruments and finally compare three selected instruments in terms of luminance and color. Second, present an application of minimal sampling approach to reconstruct dense in-plane geometries based on a sparse set of measured geometries. As this approach relies on properties of a created PCA basis, we show how one can optimize sparse directions for specific pigment types or coating systems. As the span of our tested coatings is limited, we present this optimization method as an application showcase rather than a reference directions.

Keywords: effect coatings, appearance capturing, instrument, gonireflectometer, measurement

1. Introduction

A proper and reliable characterization of coatings containing different effect pigments [1] like metallics, pearls or diffractive is of high interest for designers as well as to the complete coatings and plastics industry, especially when it comes to quality control. The industrial quality control instruments tend to perform this task by capturing very limited number of geometries by affordable and portable package, that can be used for various types of surface analysis. In this paper we ask several questions: Which set of geometries or device works the best for effect coatings characterization? Can we find new directions optimized for characterization and reconstruction of specific types of coatings?

Our findings are reported in the following sections. Section 2 briefly overviews the history of geometries for coatings characterization and instruments used in the last two decades. Section 3 presents a side-by-side comparison of the latest instruments in terms of luminance and color. Section 4 proposes a method of dense in-plane reconstruction out of a sparse set of geometries, which can be simultaneously optimized for the test

dataset. Section 5 provides possible directions of future research and concludes the paper.

2. Measurement geometries in industry

In the coating industry the past decades were marked by development and the wide usage of special effect pigments[1]. This evolved in a great expansion of available appearance variation needed to be uniquely characterized. First methodologies used in the seventies and eighties suggested only between two and four geometries that were sufficient for the characterization of coatings showing solid color [2]. With the onset of effect pigments, more geometries turned to be necessary and development converged to the acceptance of standard ASTM E 2539–08 [3] that was later on further extended to ASTM E 2539–12 [4]. Fig. 2 depicts ASTM E 2539–08 geometries (a) due to scattering or orientation, (b) due to interference.

Several industrial instruments have been introduced in the last three decades. Selected six of them are shown in Fig. 1 including geometries they capture. Note that normal arrows represent illumination directions and bold arrows represent pick-up directions, while colors link together individual groups of bidirectional pairs.

Email addresses: filipj@utia.cas.cz (Jiří Filip),

frank.maile@schlenk.de (Frank J. Maile)

URL: <http://staff.utia.cas.cz/filip> (Jiří Filip),

<http://www.schlenk.de> (Frank J. Maile)

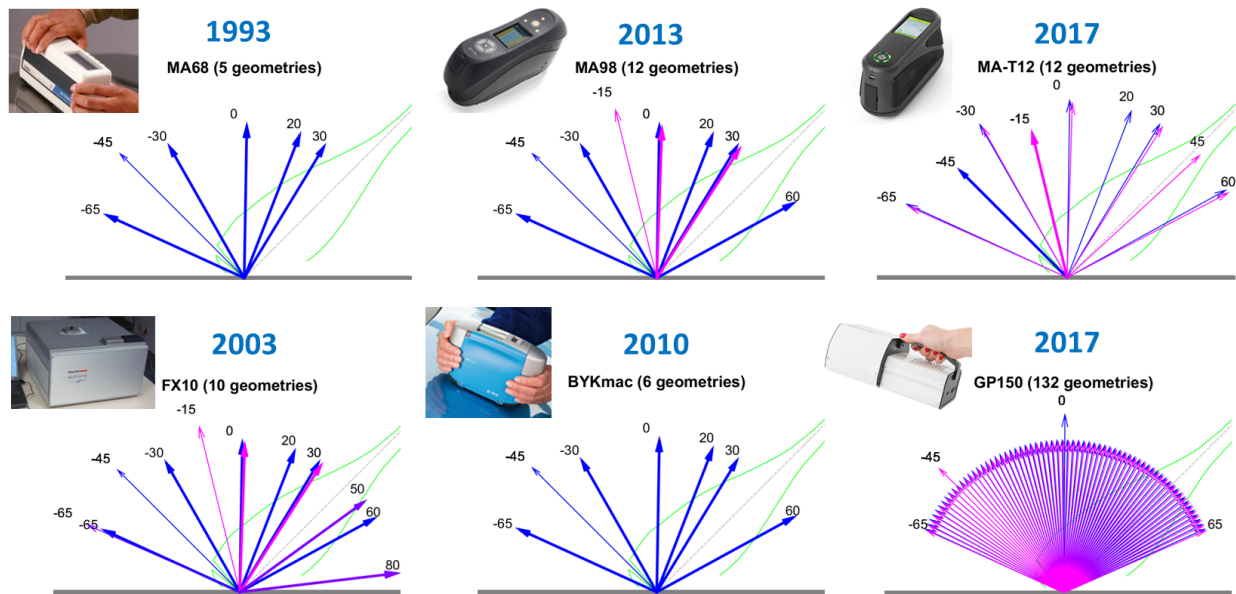


Figure 1: Geometries implemented by commercial industrial instruments in the past two decades.

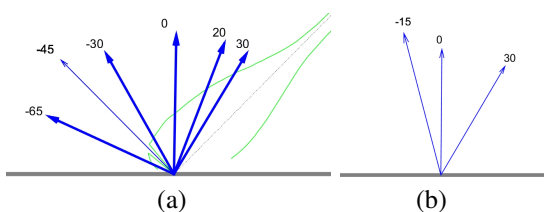


Figure 2: ASTM Geometries (E 2539-08) for (a) color due to scattering or orientation (45° : asp 15° , 25° , 45° , 75° , 110°), (b) color range due to interference (15° : asp 15° , asp- 15°).

The first instrument is MA 68 by X-Rite implementing five ASTM in-plane scattering geometries. The next device is the Multi FX-10 by DataColor capturing additional two ASTM interference geometries and two geometries for illumination at 65° . BYKmac by Gardner implements five ASTM in-plane scattering geometries plus an additional geometry 45° asp- 15° . This device was pioneering the effect coating texture analysis represented by two proprietary texture features: *graininess* obtained for diffuse illumination, and *sparkliness* obtained for three directional illuminations. Further, release of MA-98 by X-Rite brought ability to measure additional four out-of-plane geometries, however texture analysis was missing. Such analysis has been included to recent instrument MA-T12 capturing ASTM geometries plus additional four samples for illumination at 15° . MA-T12 used the Helmholtz reciprocity and substitutes incoming and outgoing directions. There-

fore, it features two pickup angles: at 15° and 45° and six illumination directions defined by ASTM geometries. Due to this, the illumination sparkliness is evaluated for viewing angle 15° and six illumination directions. Finally, the quite new instrument GP150 by See- Lab allows to capture arbitrary viewing direction (in two degree steps) in range $\pm 65^\circ$ for illuminants at 0° and 45° , however, currently without option of texture analysis.

When it comes to practical measurements of effect coatings, all portable instruments are facing two main challenges. The first one, is a very short distance between the measured sample and the sensor (typically less than 10 cm). Such a short distance in combination of sensing area of diameter 1-2 cm result in varying viewing angles acquired by the sensor. This becomes a problem when approaching the specular reflection with high intensity values, where the intensity of specular highlights is not captured accurately but as an average value across a range of viewing angles. The problems as a consequence manifests itself in lower intensity of specular peak luminance value and it higher width as demonstrated in Fig. 3-a depicting the linear plot of in-plane values obtained by our goniometer setup for view 45° and variable illumination directions. For a fixed camera distance, we obtained decreasing values of specular peak intensity with increasing size of captured sample area used for luminance values averaging.

The second challenge, is the instrument alignment ow-

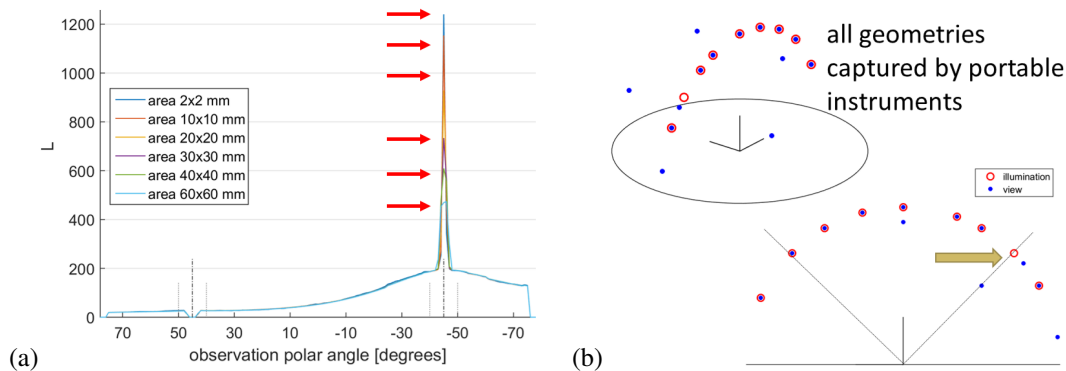


Figure 3: (a) Impact of the sample size for fixed sensor distance, (b) all geometries captured by industrial devices.

ing to the material sample. An accurate alignment is difficult even for ideally planar samples where misalignment of specular highlights from the ideal specular reflection angle withing several degrees cannot be practically avoided. We believe that this is one of the reasons while the majority of instruments do not capture values near specular angles as shown in Fig. 3-b illustrating all bidirectional geometries captured by industrial instruments described in this section (except GP150 whose performance in capturing near specular data is discussed in the next section).

3. A comparison of three instruments

In this section we compare three industrial instruments: BYKmac, MA-T12 and GP150 in terms of luminance and color. As a test set for comparison, we used 10 samples featuring four types of pigments: ultra-thin pigment (UTP), diffractive pigment of three different mean particle sizes, vacuum-metallized pigment (VMP), and aluminum pigment as shown in Fig. 4. As a reference for

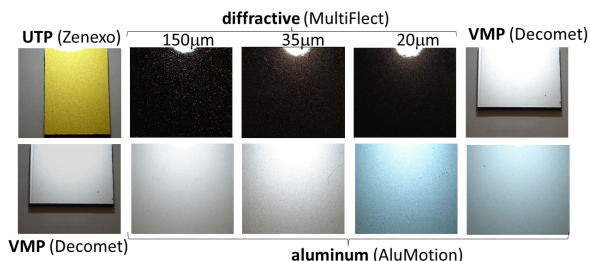


Figure 4: The set of 10 samples of effect coatings used for our comparison.

values captured by the compared devices we captured in-plane geometries for fixed view 45° and illumination

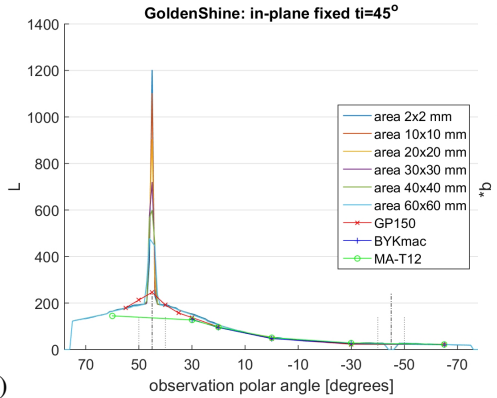
direction $\pm 75^\circ$ in one degree steps using the UTIA gonireflectometr [5].

Figures 5 and 6 compare performance of individual instruments in luminance channels (left), a-b channels (middle), and in the inter-instrument correlation. Luminance plots show the reference measurements (for variable sample pick-up area) as solid outlines, results of GP150 as red-line, BYKmac as blue line and MA-T12 as green line. The a-b charts show a-b values measured by reference and compared instruments connected by a dashed line for individual ASTM geometries. The correlation plot illustrates inter-device Pearson correlation values across five ASTM geometries, where width of lines correspond to correlation values in range (-1,1) with green/red values indicating positive/negative correlation, respectively. Note that we captured five ASTM geometries by all devices. Additionally, for MA-T12 we captured also the geometry 45asp- 15° although BYKmac allows the same. In contrast, GP150 allows capturing much more geometries than the other two devices, thus we included five specular and near specular values.

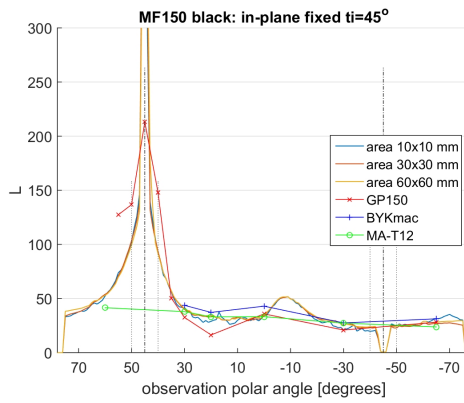
Fig 5 shows the comparison on (a) the UTP pigment, (b) diffractive pigment $D_{50}=150 \mu\text{m}$, (c) diffractive pigment $D_{50}=35 \mu\text{m}$. In all cases, for the instrument GP150 we can observe the effect of small sensor distance resulting in a decreased captured intensity of specular highlights and its increased width (when compared with the reference data).

While for the UTP pigment all devices performed similarly in terms of luminance and color, for the diffractive pigment we could observe deviation especially for GP150 and for mean particle size $150 \mu\text{m}$ also for BYKmac. Therefore, for the diffractive pigment one can observe significantly higher correlation between MA-T12 and the BYKmac.

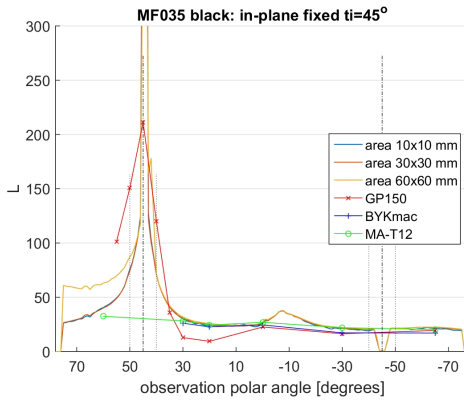
luminance



(a)

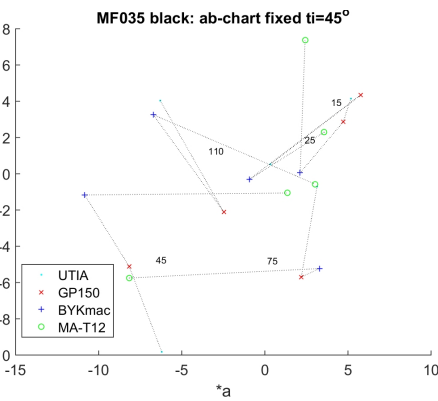
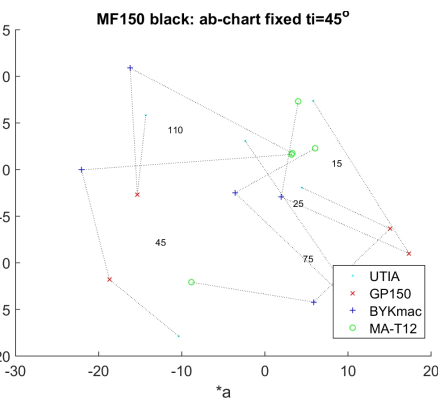
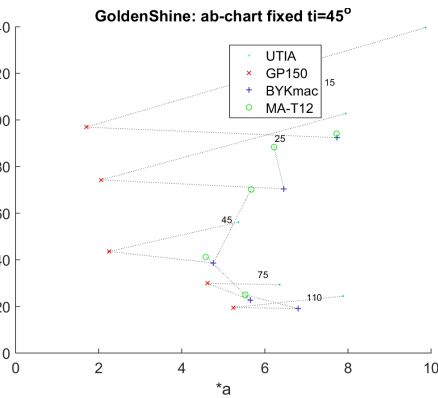


(b)



(c)

a-b chart



correlations

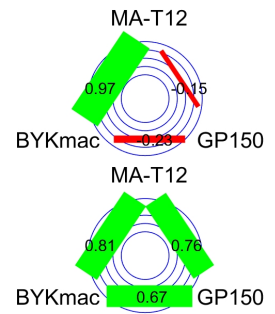
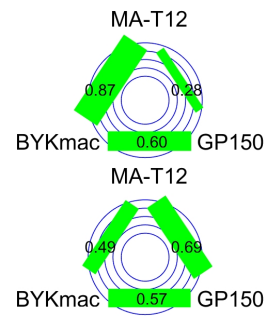
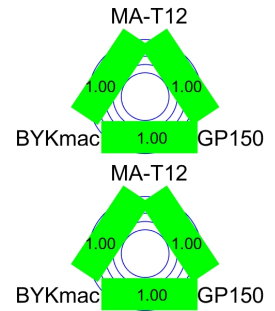


Figure 5: Luminance and a-b charts supplemented with inter-device correlation computed across ASTM geometries: (a) UTP, (b) diffractive $D_{50}=150\mu\text{m}$, (c) diffractive $D_{50}=35\mu\text{m}$.

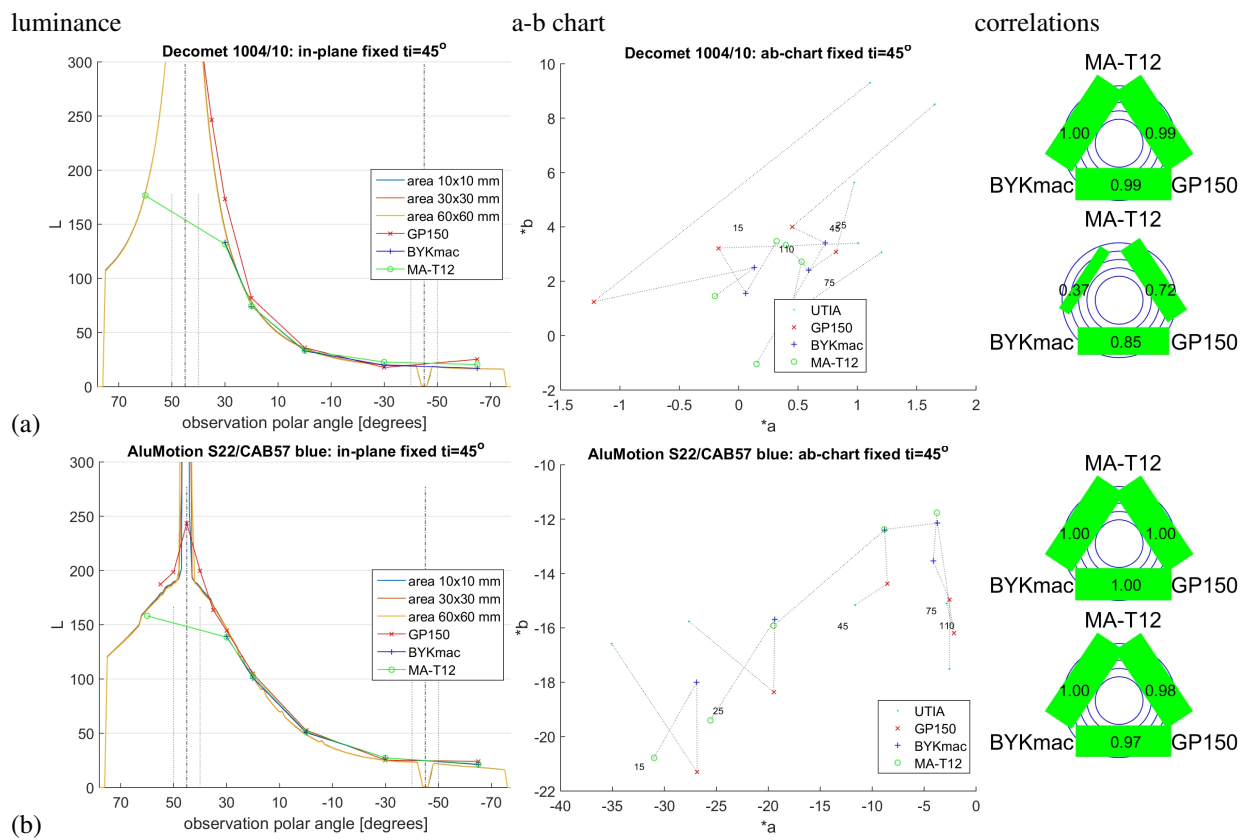


Figure 6: Luminance and a-b charts supplemented with inter-device correlation computed across ASTM geometries: (a) VMP, (b) aluminum (blue-tint).

Fig 6 brings a comparison for the (a) VMP pigment, (b) aluminum pigment (in the blue-tint). In both cases we can observe good correlation between all instruments in luminance. Generally, the correlation in ab channels are significantly lower especially for achromatic samples (diffractive, VMP) where a-b values are typically very low representing more or less noise readings.

Finally, Fig. 7 shows correlations in (a) luminance, (b) a-b channels averaged across all ten tested coating samples. Our results suggest that in luminance a slightly higher correlation value were between BYKmac and MA-T12, while for this configuration there is a slightly lower correlation in a-b channels.

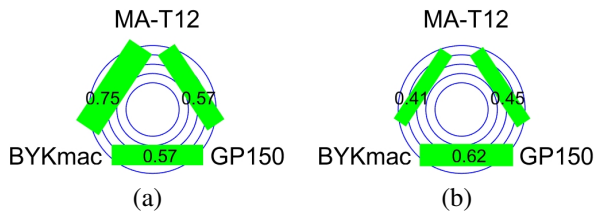


Figure 7: Correlations across ASTM geometries averaged across all tested materials for: (a) luminance, (b) a-b channels.

Generally, we can conclude that all tested instruments deliver very good performance, especially in luminance analysis, across different effect pigments.

4. Dense in-plane reconstruction from sparse optimized directions

In the second part of the paper, we present a method of dense in-plane data reconstruction using sparse and optimized geometries. Our approach is inspired by the one in [6], allowing to substitute tedious sampling of bidirectional pairs during BRDF [7] acquisition by using simple geometry, e.g. industrial reflectometers, multiple-times with different orientation over coating surface. Here, we consider only in-plane geometry and fixed viewing angle 45° and optimize illumination polar angles.

As the method relies on database of basis functions, a representative dataset of in-plane coatings behaviour is necessary. To this end, we collected 47 coating samples (see Fig. 11) of 7 different pigment types: 16 diffractive, 7 aluminum, 9 mica, 7 combination of aluminum and mica, 4 ultra-thin pigment (UTP), 1 vacuum metalized pigment (VMP). These coatings can be also divided to three categories based on the used coating system: solventborne, powder, waterborne.



Figure 8: An overview of 47 coatings used as input to our reconstruction method.

For each material, 151 in-plane geometries are captured for fixed viewing illumination polar angle 45° and varying illumination polar angles ranging $(-75^\circ, 75^\circ)$ in one degree steps as shown in Fig. 9-a. Note that 10 near retro-reflective values are missing due to camera view occlusion by the illumination source. For each geometry a high-dynamic range RGB image is captured. To get correct information on near-specular behavior, only the area within light specular reflection (250×250 pixels) is picked up. To further increase data variability within each coating, we divided the area into four regions as shown in Fig. 9-b.

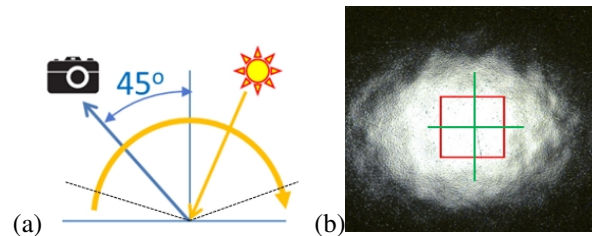


Figure 9: A scheme of captured angular geometries (a), a location of sampled area within specular highlight used for in-plane data collection (b).

Then each region is treated as separate data vector. As the dataset contains 47 coatings, we obtain 188 data vectors.

Once the dataset is prepared, we perform a linear factorization to obtain a set of basis function that can be used for reconstruction of any in-plane geometry. Once the basis functions are generated, we use eigenvectors to optimize the required number of geometries. More information on this semi-random process relying on iterative computing of conditional numbers of geometries subsets can be found in [8] and [6].

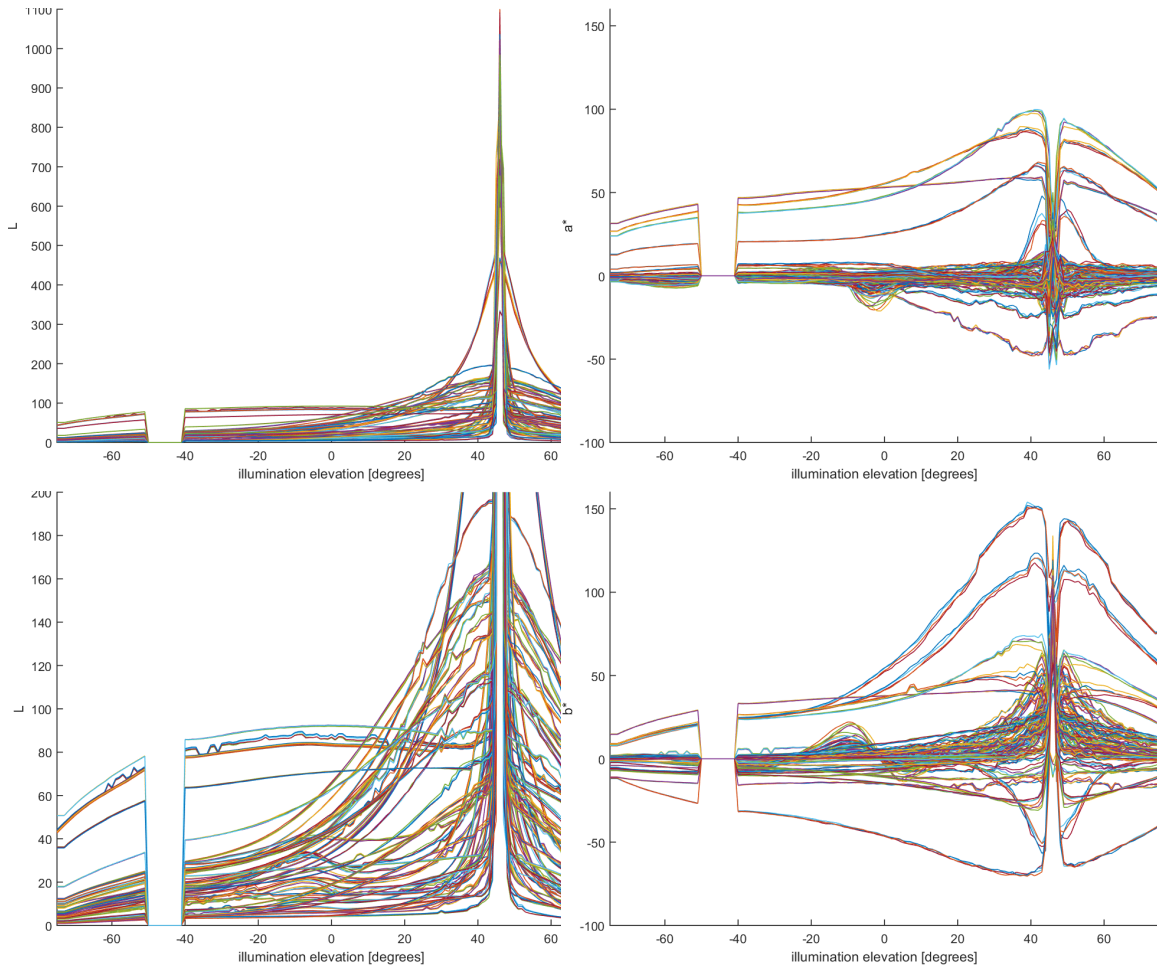


Figure 10: An overview of 188 measured data vectors in L (left-top, left-bottom), a, b (right) channels.

Finally, when we need to reconstruct in-plane behavior of material which is not in the dataset, we capture this material L-a-b values only in these sparse geometries (possibly using an industrial spectrophotometer) and obtain dense values for 151 geometries by combina-

tion of the basis functions. It is important to note that, in order to get this method working well, the training dataset should contain similar types of coatings that are being reconstructed, i.e., in other words, the database should contain similar in-plane profiles to those of query materials.

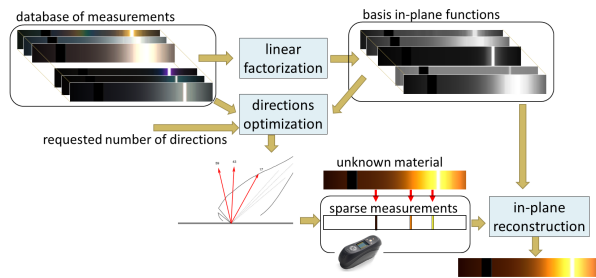


Figure 11: A scheme of the proposed dense in-plane method from optimized sparse geometries.

The method optimizes the required sparse number of geometries. However, as explained in the previous section the data near specular reflection can suffer in term of accuracy and/or alignment so we might want to exclude them from the optimization. When we fixed a number of directions to be optimized to six while increasing size of restricted area from 0° to 15° , we observe that there was always one of optimized direction close to boundary of restricted area. This suggests that near specular area bring important information for data reconstruction process. Therefore, we also applied a feature selection technique to evaluate importance of in-

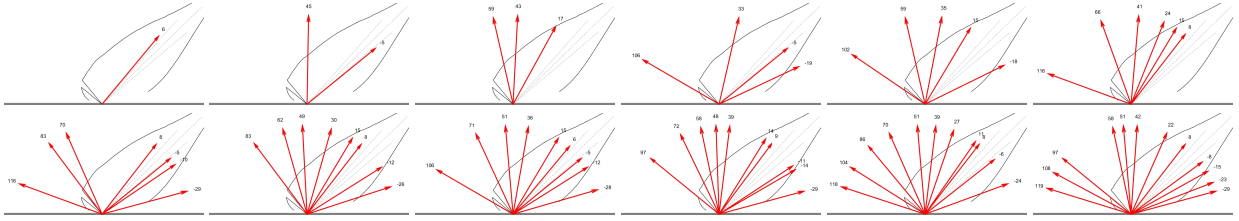


Figure 12: Optimized 1–12 illumination geometries for view 45° .

dividual dense in-plane geometries for classification of pigment type. Here we observed a significant drop of importance for features close ± 3 degrees from a specular reflection. Therefore, in further experiments we restricted optimized directions to be more than 4 degrees from specular reflection.

Fig. 14 illustrates 1–12 optimized geometries. We can observe that one or more optimized directions are almost always near restricted boundary of specular reflection, which indicates the importance of specular data.

The proposed method uses the basis functions and optimized directions to reconstruct data in all L-a-b channels. We visualize the quality of reconstruction by direct comparison to the reference measured values as shown in Fig. 13. In general, the reconstruction works well if there is not visual difference between upper and bottom part of the image.

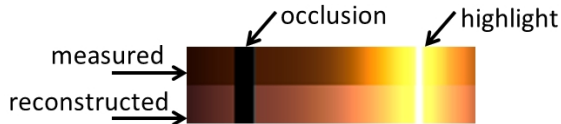


Figure 13: A scheme of comparison of reference (top) and reconstructed (bottom) dense in-plane geometry (viewing angle 45° , illumination polar angle $-75^\circ \dots 75^\circ$).

Fig. 14 shows an example of performance of the proposed method on coatings representing different pigment types for 1, 3, 6, 9 and 12 optimized geometries. We can see that the method performs well even using 6 directions only, with the exceptions of diffractive and color-shifting pigments. While for the former it is due to a specific complex chromatic behavior, for the latter it is due to missing basis functions of such behavior in the dataset (there was just one color-shift paint in the training dataset).

We also assessed the reconstruction error computationally by means of peak-signal-to-noise ratio (PSNR). The better the quality, the higher the PSNR value.

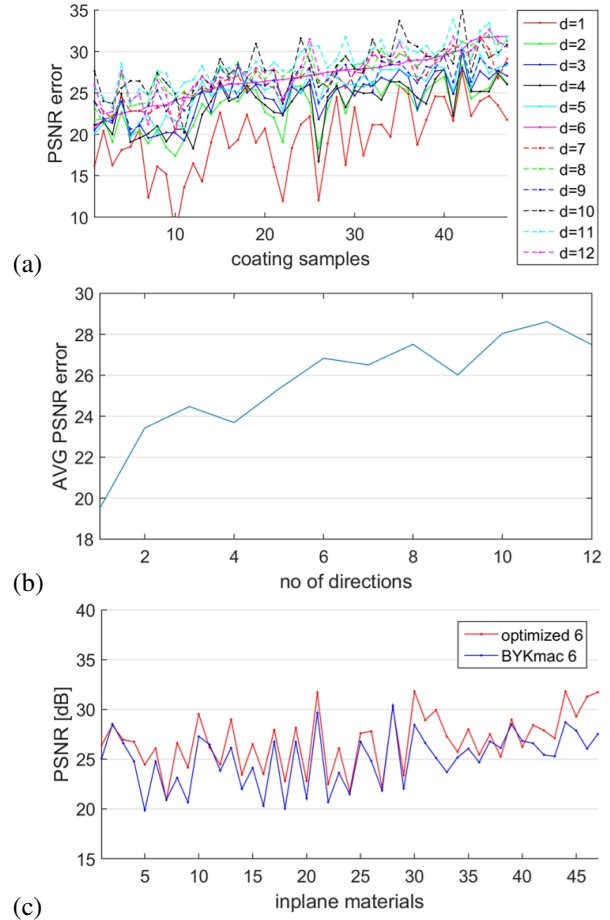


Figure 15: PSNR reconstruction errors for (a) individual materials, (b) averaged. (c) Compares performance of 6 optimized directions to ASTM E2339 geometries including 45asp-15.

Fig. 15-a depicts PSNR values for the reconstruction of individual coatings for variable number of sparse geometries (1–12). The materials are ordered based on PSNR for 6 geometries, therefore, its graph is monotonous. Here we observe that 6 geometries provide a good trade-off between reconstruction quality and number of geometries. This observation is confirmed by averaging PSNR across all tested coatings

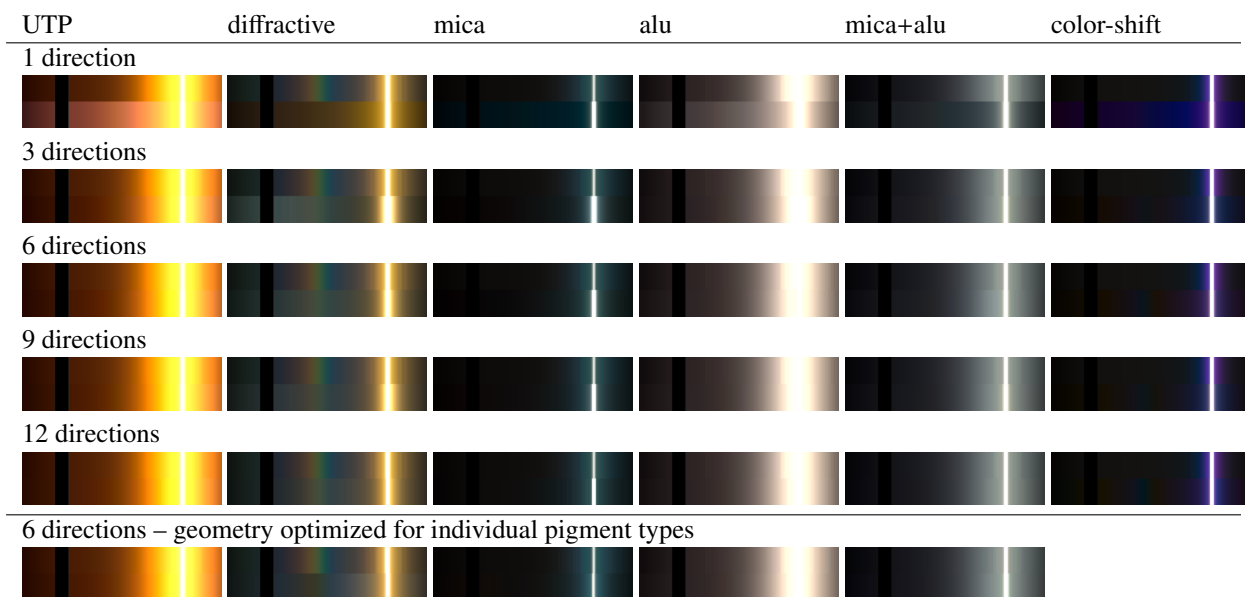


Figure 14: In-plane dense reconstruction using variable number of directions for different pigment types.

in Fig. 15-b. Finally, we compared reconstruction using optimized 6 geometries with 5 geometries of ASTM E2339 standard including 45asp-15. Here, we observe better performance of the optimized directions.

One can also improve the performance of this method by optimizing geometries for specific pigment types, coating systems, etc. simply by its fitting to corresponding subset of data only. Such optimized directions are shown in Fig. 16, where we can see that optimization for specific pigment types and coating systems improved reconstruction error for these data subsets. Note the different shapes of average specular lobes (green outline) for different pigments and coating systems.

The bottom line in Fig. 14 demonstrates the improvement obtained by illumination geometries optimization for individual pigment types using six directions.

Discussion – The proposed method allows reconstruction of dense in-plane behavior for fixed observation 45° polar and variable illumination directions based on sparse sampling geometries. The sparse data can be collected by a goniometer (using optimized geometries) or by an industrial gonireflectometer (using standard ASTM geometries). Our method depends on the training dataset which should represent data going to be reconstructed. In our study, only 47 coatings were used. This number might be insufficient to represent all variability of effect coatings state space. Therefore, we suggest the reader to perceive our method more as an ap-

plied tool rather than a final recommendation of optimal geometries to be practically used. This approach can be easily extended to optimize not only illumination elevation angles but also bidirectional pairs, or even out-of-plane bidirectional pairs as shown in [6]. Finally, captured in-plane data can be used for approximate real-time coating visualization.

5. Conclusions

Contributions of this paper are twofold.

First, it presents the comparison of three industrial gonireflectometers in terms of luminance and color on 10 effect coating samples and present inter-device correlations over ASTM geometries.

Second, we propose an approach for convenient and fast reconstruction of data for dense in-plane geometries from sparse samples, which relies on a representative database of captured coatings. We have shown that 6 geometries is enough for reasonable luminance and color reconstruction and that these geometries can be successfully optimized for different pigment types and coating systems.

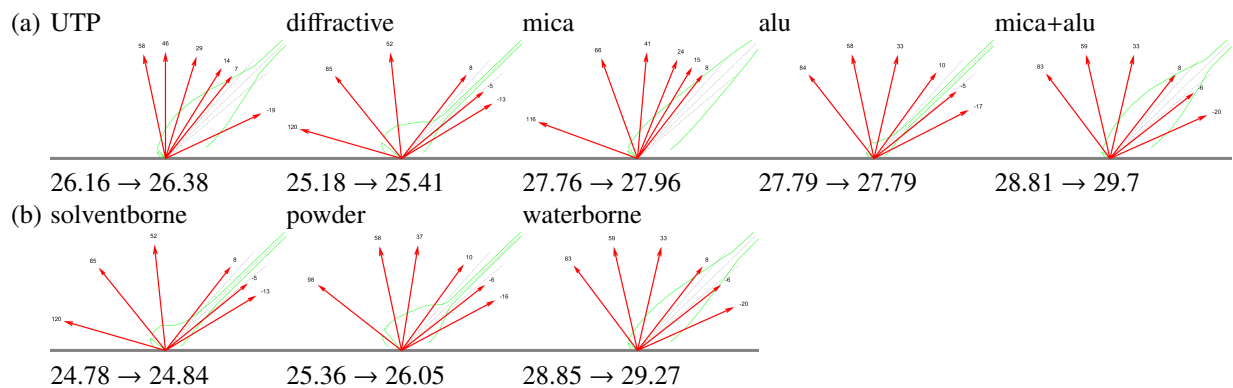


Figure 16: The 6 geometries optimized for: (a) pigment types, (b) coating systems ($s_r = 4$), including change of PSNR values.

Acknowledgments

We would like to thank the advisory board for inviting us to present our work. We gratefully acknowledge the great support by Dr. Radomír Vávra, Dr. Petr Somol, Martina Kolařová and Prof. Michal Haindl (UTIA CAS, v.v.i.) for their help regarding data capturing and overall support.

This research has been supported by the Czech Science Foundation grant GA17-18407S (*Perceptually Optimized Measurement of Material Appearance*).

6. References

- [1] F. J. Maile, G. Pfaff, P. Reynders, Effect pigment – past, present and future, *Progress in Organic Coatings* 54 (3) (2005) 150–163.
- [2] C. S. McCanny, Observation and measurement of the appearance of metallic materials. part. 1. macro appearance, *COLOR research and applications* 21 (4) (1996) 292–304.
- [3] A. E2539-08, Standard practice for multiangle color measurement of interference pigments, ASTM International (2008).
- [4] A. E2539-12, Standard practice for multiangle color measurement of interference pigments, ASTM International.
- [5] J. Filip, R. Vávra, M. Haindl, P. Zid, M. Krupicka, V. Havran, BRDF slices: Accurate adaptive anisotropic appearance acquisition, in: *In proceedings of the 26th IEEE Conference on Computer Vision and Pattern Recognition, CVPR 2013*, 2013, pp. 4321–4326.
- [6] R. Vávra, J. Filip, Minimal sampling for effective acquisition of anisotropic brdfs, *Computer Graphics Forum* (2016) 299–309.
- [7] F. Nicodemus, J. Richmond, J. Hsia, I. Ginsburg, T. Limperis, Geometrical considerations and nomenclature for reflectance, *NBS Monograph* 160 (1977) 1–52.
- [8] J. Nielsen, H. Jensen, R. Ramamoorthi, On optimal, minimal brdf sampling for reflectance acquisition, *ACM Transactions on Graphics* 34 (6) (2015) 186:1–186:11.